NJC

New Journal of Chemistry

A journal for new directions in chemistry

Accepted Manuscript

Volume 42
Number 6
21 March 2018
Pages 3963-4776

NJC

New Journal of Chemistry
rsc.li/njc

A journal for new directions in chemistry

ISSN 1144-2546

PAPER
Chechia Hu, Tzu-Jen Lin *et al*
Yellowish and blue luminescent graphene oxide quantum dots
prepared via a microwave-assisted hydrothermal route using
H2O2 and KMnO4 as oxidizing agents

ROYAL SOCIETY
OF CHEMISTRY

CNrs
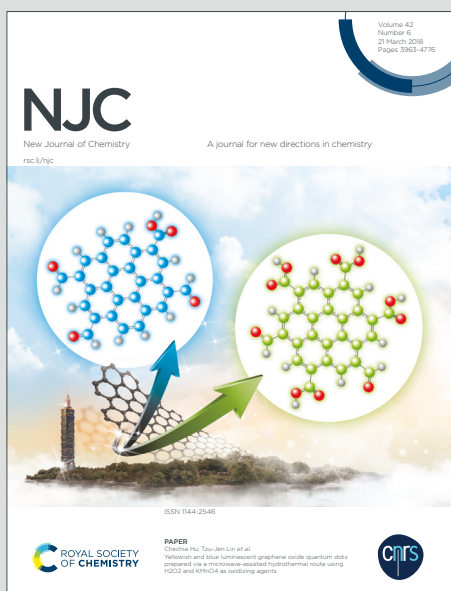
This is an Accepted Manuscript, which has been through the Royal Society of Chemistry peer review process and has been accepted for publication.

Accepted Manuscripts are published online shortly after acceptance, before technical editing, formatting and proof reading. Using this free service, authors can make their results available to the community, in citable form, before we publish the edited article. We will replace this Accepted Manuscript with the edited and formatted Advance Article as soon as it is available.

You can find more information about Accepted Manuscripts in the Information for Authors.

Please note that technical editing may introduce minor changes to the text and/or graphics, which may alter content. The journal's standard Terms & Conditions and the Ethical guidelines still apply. In no event shall the Royal Society of Chemistry be held responsible for any errors or omissions in this Accepted Manuscript or any consequences arising from the use of any information it contains.

ROYAL SOCIETY
OF CHEMISTRY

rsc.li/njc

ARTICLE

Dual adsorbent-photocatalytic Keratin-TiO₂ nanocomposite for trimethoprim removal from wastewater.

María Emilia Villanueva,[a,b,c] Mayra Puca,[a] Jonas Pérez Bravo, [b,d] Jonathan Bafico,[a] Viviana Campo Dall Orto[a,b] and Guillermo Javier Copello [*a,b]

Abstract Trimethoprim is an emergent pollutant that has been found in ground water in alarming concentrations. Thus, the development of economical and efficient advanced water treatment technologies is crucially needed. In this paper, a keratin hydrogel with immersed TiO₂ nanoparticles (nTiO₂) was developed. The material was characterized by FT-IR and FT-Raman showing that a physical interaction between nTiO₂ and keratin hydrogel took place. Dielectric spectroscopy confirmed the influence of this interaction with the keratin structure. Swelling studies showed that it depended on the media pH, being higher at basic pH values. Photocurrent measurements revealed an enhanced photocurrent of the hydrogels which may be due to the improved transition of photogenerated carriers via the porous network structure. The model pollutant was trimethoprim, an emerging pollutant. These hydrogels showed the ability to adsorb and degrade trimethoprim in the presence of simulated solar light in batch conditions for at least four cycles with no significant decrease in the efficiency. Experimental variables (time, temperature, pH) were studied in order to characterize the material adsorption and photodegradation performance, concluding that the temperature is a main variable to consider in the adsorption process.

Introduction

The anthropogenic activities constantly produce emerging pollutants which enter the environment and can be found in groundwater, surface water, municipal wastewater, drinking water, and food sources. They generally are organic compounds such as pharmaceuticals, antibiotics, hormones, endocrine disruptors, perfluorinated molecules, disinfection byproducts, sunscreens, flame retardants, algal toxins, dioxane or pesticides and their degradation byproducts.[1–3] These chemicals are not commonly controlled but have the potential to get in the environment and cause negative ecological and human health effects. In addition, they are persistent. Since rates of effluent introduction often exceed their half-lives in a receiving ecosystem, they have the tendency to accumulate in living tissues thus entering the food chain and synergistic toxicity regularly occur associated to their presence.[4]

The presence of antibiotics, such as trimethoprim, in natural water affects the environment in several ways. First, the presence of these kind of compounds alter the natural flora and may provoke bacterial resistance. [5–7] In this context, the development of

economical and efficient advanced water treatment technologies is crucially needed.

In recent years, advanced oxidation technologies (AOT), including photocatalytic degradation in heterogeneous phase, became attractive and important as they have great potential to contribute to wastewater remediation [8–10]. The photocatalytic process can completely mineralize organic compounds to water, carbon dioxide and other inorganic compounds without causing secondary contamination.[11,12] For instance, trimethoprim has been mineralized by TiO₂ nanoparticles treatment [13,14]. One of the most important aspects of photocatalysis is the selection of materials. Semiconductors such as TiO₂ are usually used as a photocatalyst in the literature, since they are relatively inexpensive and highly effective [9,15,16]. The photocatalytic activity of TiO₂ depends on several parameters, such as the crystal forms, percent crystallinity, doping materials, surface area, and the density of surface hydroxyl groups.[17] TiO₂ powder (Degussa, P-25), which is a standard material in the field of photocatalytic reactions, contains anatase and rutile phases in a ratio of about 3 : 1. Photocatalytic degradation of pollutants is inefficient on pure anatase and rutile powders. However, the reaction is very efficient on a mixture of anatase and rutile particles. [18] Unluckily, the implementation of these nanomaterials in large water volumes is not easily accomplished. Decantation and/or filtration is needed to separate the nanophotocatalyst from the effluent. Thus, their inclusion within a 3D matrix simplifies the operational aspects, such as collection and separation of the materials from the liquid media. In addition, the matrix can contribute to the remediation process if it shows affinity for the target contaminant. In these nanocomposites both adsorption and degradation of the pollutants take place making this technology one of the most auspicious alternatives [19–22]. Keratin is considered an economical and high accessible biosorbent. It can be

a. Universidad de Buenos Aires (UBA), Facultad de Farmacia y Bioquímica, Departamento de Química Analítica y Fisicoquímica, (UBA), Junín 956, C1113AAD, Buenos Aires, Argentina

b.CONICET – Universidad de Buenos Aires (UBA). Instituto de Química y Metabolismo del Fármaco (IQUIMEFA), Buenos Aires, Argentina;

c.Universidad Nacional de Luján (UNLu) Departamento de Ciencias Básicas, Ruta 5 y 7 Luján, Buenos Aires, Argentina;

d.CONICET – Universidad de Buenos Aires (UBA). Instituto de Tecnología de Polímeros y Nanotecnología (ITPN), Buenos Aires, Argentina.

* gcopello@ffyb.uba.ar.

obtained from waste materials of the livestock and poultry industry such as hair, wool, hooves, horns, feathers, etc [23–25]. Generally, the obtained keratin materials (sponge or film structures) have good flexibility but poor mechanical properties. Therefore, keratin have been conjugated with other polymers such as chitosan, gelatin, and silk fibroin, generating keratin-based hybrid materials [26–28]. This protein has shown biosorbent capacity [29–31], thus, new materials taking advantage of this quality were found in the literature. For example, with the incorporation of nanomaterials, a reinforcement of the structure [32,33] and other properties such as catalytic or photocatalytic activity, were observed. [34–36]

The aim of this study was to develop a system for trimethoprim remediation in waste waters using a keratin hydrogel and TiO_2 nanoparticles ($nTiO_2$). The material was characterized by FT-IR, FT-Raman, photocurrent measurements and dielectrical spectroscopy in order to analyse the nanopartides – polymer interactions. Besides, these hydrogels showed the ability to adsorb and degrade trimethoprim in the presence of simulated solar light in batch conditions. Experimental variables (time, temperature, pH) were studied in order to characterize the material photocatalytic performance. The principal goal of this work was to demonstrate the suitability and reusability of photocatalytic $nTiO_2$ immobilized on a keratin hydrogel for the degradation of trimethoprim.

Materials and Methods

Materials

Sodium hydroxide, Potassium hydrogen phosphate and Potassium dihydrogen phosphate were purchased from Anedra (Argentina). Ethanol 96% was acquired from Soria (Avellaneda, Argentina). Ethyl Acetate was purchased from Sintorgan (Argentina), TiO_2 nanoparticles (AEROXIDE TiO_2 P-25, Evonik) were kindly donated by Evonik Degussa Argentina SA. Trimethoprim was acquired in Saporiti (Argentina). All other reagents were of analytical grade. Whole cow's horns (*Bos taurus*, Hereford) were kindly donated by Frigorina (La Plata, Buenos Aires, Argentina) and used as keratin source.

Hydrogel synthesis

Horn was pulverized and sieved through a 250 μm sieve. After that, the horn powder was rinsed three times with distilled water and with ethyl acetate to remove fat. Then, the powder was dried at 37°C overnight. A 18.0 mL dilution of 0.3 N NaOH in Ethanol (25 mL) was added to 1 g of the keratin powder. The mixture was left at 45 °C for 4 h. Afterwards, it was mixed with different amounts of $nTiO_2$ (in order to obtain a 1, 5 and 10 % w/w $nTiO_2$ keratin hydrogels), the mixtures were homogenized through a syringe and left until complete dryness at 45 °C. The final product was a dry block of keratin that was easily hydrated in water to form the hydrogel and it was named K-TiO_2 1%, K-TiO_2 5% and K-TiO_2 10%. A control without the addition of the nanoparticles was prepared and named K. The obtained keratin blocks were thoroughly rinsed with deionized water in order to remove all NaOH residue.

Characterization

Spectroscopic characterization

ATR-FTIR (diamond attenuated total reflectance) of keratin materials were recorded using a Nicolet iS50 Advanced Spectrometer (Thermo Scientific). ATR-FTIR spectra were recorded with 32 scans and a resolution of 4 cm^{-1}. FT-Raman spectra were acquired with an excitation laser beam of 1064 nm, 0.25W laser power, resolution of 4 cm^{-1}, 400 scans. All samples were previously dried for 24 h at 60 °C to avoid water related bands interference. Amide I band (1690-1640 cm^{-1}) was deconvoluted for the analysis of the α-helix (1655 cm^{-1}) and β-sheets (1679 cm^{-1}) components. Spectral baselines were set between 1750 and 1503 cm^{-1}, taking in consideration the overlapping of the ν(C=C) olefinic band (1604 cm^{-1}) with the amide I band. Spectra decomposition was performed using Fityk software [37] assuming a Lorentzian shape for narrow peaks (α-helix and olefinic band) and a Gaussian form for broad peaks (β-sheets) [38].

X-ray diffraction (XRD) patterns from keratin and composites were obtained using a Rigaku diffractometer with Bragg Brentano geometry and CuKα radiation (*l* = 0.1542 nm, 40 kV, 20 mA) in the range of 2θ = 3 – 50 ° at a scanning rate of 1 °/min and a scan step of 0.05 °. Measurements were performed at ambient conditions.

Swelling behavior

In order to assess the swelling behavior of the materials, 0.0500 ± 0.0020 g of a keratin block were equilibrated in 10 mM phosphate solutions ranging from pH 4 to pH 8. After equilibrium was reached, the hydrogels were removed from the solution and accurately weighted.

Dielectric spectroscopy

Dielectric spectroscopy spectra were acquired using a Palm Sense 4 electrochemical workstation (Netherlands). Measurements were carried out in the frequency range 0.01 Hz-1 MHz at room temperature. Glassy carbon (diameter: 3mm) and graphite electrodes were employed as the working and the counter electrode respectively. Hydrogels with a swelled thickness of 0.55 mm were used as test pieces.

Scanning electron microscope

Scanning Electron Microscopy images were obtained using a Zeiss SUPRA 40 Scanning Electron Microscope. The samples were previously coated with gold.

Trimethoprim quantification

The quantification was performed using a HPLC system consisting in a Hewlett Packard 1050 pump with a 20 μL injection loop, a Supelco column RP 18 150 x 0.4 mm mobile and a Pharmacía-LKB UV detector. Separation was performed at room temperature by isocratic elution of the analyte using a mobile phase containing acetonitrile-water (40:60) and a flow rate of 1 mL/ min.

Trimethoprim adsorption in dark conditions

Trimethoprim adsorption was evaluated in dark conditions at different pH values at 25 °C. A weight of 0.0500 ± 0.0020 g of K, K-TiO_2 10% and TiO_2 were left in contact with 5.00 mL of a 0.172 mM trimethoprim solution at pH 4, 5, 6, 7 and 8 (10 mM phosphate solutions). After 18 h, 0.050 mL of supernatant were collected, centrifuged and reserved for quantification.

The influence of temperature was also studied by weighting 0.0500 ± 0.0020 g of K and K-TiO_2 10% were left in contact with a 0.172

mM trimethoprim solution at different temperature conditions (25, 45 and 60 °C). After a certain amount of time, 0.050 mL were collected, centrifuged and reserved for quantification. A trimethoprim solution was also exposed at different temperatures as a control.

Photocatalytic Experiments

The photocatalytic activity was evaluated by the decomposition of the trimethoprim under a simulated solar light using a Xenon lamp. The irradiation intensity for all assays was 28000 lux, with less than 5% variation. Aqueous solutions of trimethoprim (50 mL, 0.172 mM) were placed in a vessel, and 0.0500 ± 0.0020 g of the samples were added. Prior to irradiation, the suspensions were left in the dark for 30 min. At certain time intervals, aliquots were sampled, centrifuged and reserved for quantification. This assay was conducted in different conditions in order to evaluate the materials performance. Hydrogels with different $nTiO_2$ concentrations (1 %, 5 % and 10%) were exposed to a 4 h intervals at 25°C. These samples were also exposed to 4 reuse cycles in the same conditions described above. Since the results showed a better performance for $K-TiO_2$ 10%, the following assays were performed using this nanocomposite and K as a control. Different interaction times and values of pH (4.0, 5.0, 6.0, 7.0 and 8.0) were evaluated. Solution of trimethoprim without adding any hydrogel photocatalyts was investigated in order to perform a control study under the same condition.

The influence of the pH in the trimethoprim photocatalysis by $nTiO_2$ was evaluated by placing a $nTiO_2$ suspension (50 mg/mL) in a 5.00 mL vessel with a trimethoprim solution at different pH values. The trimethoprim concentration in the control vessel was 0.172 mM and the $nTiO_2$ concentration was 1 mg/mL). The optical absorption area was 1.75 cm^2. Prior to the 4 h irradiation, the suspensions were left in the dark for 30 min.

Photocurrent

The photocurrent measurements for TiO_2, $K-TiO_2$ 10% and K samples were tested using a Palm Sense 4 electrochemical workstation (Netherlands) with a standard three-electrode system.[22] Two platinum electrodes were employed as the working and the counter electrode. Ag/AgCl electrode was used as reference electrode. The samples were milled and dispersed in deionized water (the final concentration of $nTiO_2$ in the suspensions was the same in $K-TiO_2$ 10% and TiO_2 assay). A Xenon lamp was selected as the light source.

Statistical analysis

All experiments and their corresponding measurements were conducted in triplicate under identical conditions and statistically analyzed by one-way ANOVA and Bonferroni comparison post test if ANOVA $p < 0.05$.

Results and discussions

Surface characterization and Physico-chemical properties evaluation

Figure 1 A and B showed the FT-IR spectra of the hydrogels and the $nTiO_2$. In the $nTiO_2$ spectrum the typical bands (3322 cm^{-1} and 1605 cm^{-1}) could be observed. They were assigned to the stretching vibrations of the O-H (3322 cm^{-1}) and the bending vibrations of the

adsorbed water molecules, (1605 cm^{-1}). [39,40] In the hydrogel spectra keratin characteristic bands could be found: peaks were observed at 1636 cm^{-1}, which corresponded to the vibration of the C=O bond (Amide I band), and at 1524 cm^{-1}, which corresponded to a combination of the C-N stretching and N-H deformation vibrations (Amide II) [9]. The lack of TiO_2 related bands may be due to the low concentration of the nanopartides and the low infrared absorption of the TiO_2 groups.

Figure S1, S2 and S3 (Supplementary Information) showed the FT-Raman spectra of the $nTiO_2$ and the different keratin hydrogels. In the $nTiO_2$ spectrum, the characteristic peaks could be found. The
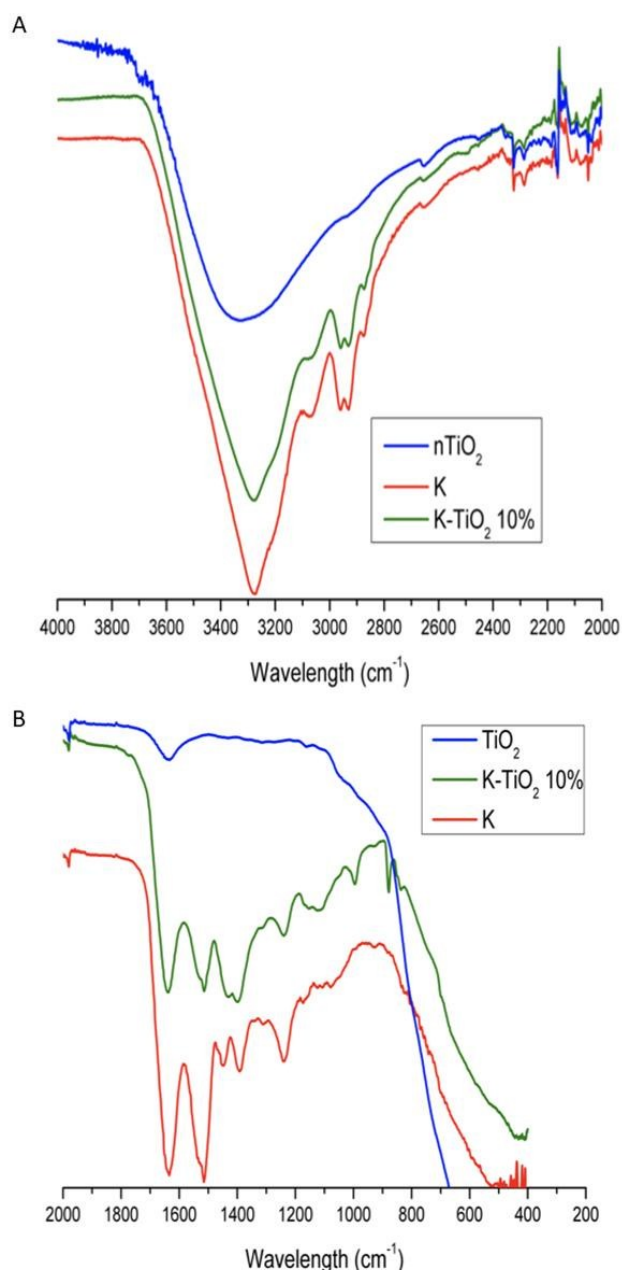

Figure 1. FT-IR spectra of $nTiO_2$, K and $K-TiO_2$ 10%.

bands at 157, 202, 406, 520, and 647 cm^{-1} were observed. These bands were assigned to the anatase phase, and they can be attributed to the five Raman-active modes of anatase phase with the symmetries of E_g, E_g, B_{1g}, A_{1g}, and E_g, respectively [41]. The FT-Raman spectra of the different hydrogels showed the characteristic bands of the keratin: the band at 1448 cm^{-1} corresponded CH$_2$-CH$_3$ bending modes. The bands at 1606 and 1668 cm^{-1} corresponded to the presence of olefinic groups and the amide I band respectively. The bands at 2937 and 3340 cm^{-1} corresponded to CH$_3$ asymmetric stretching and O-H stretching respectively.[42] The presence of nTiO$_2$ in the K-TiO$_2$ hydrogel was evidenced by the presence of the characteristic nTiO$_2$ bands. These results proved that a physical interaction between the nTiO$_2$ and the keratin hydrogel took place, since the appearance of new functionalities was not observed. Also, as can be seen from the comparison of the Amide I band of the K and the K-TiO$_2$ spectra, a conformational change was induced by the presence of the nanoparticles (Figure S4). This band accounted for the ν(C=O) stretching present in the peptide bond. Since not all peptides presented the same conformation and chemical interactions, the symmetry of this band was susceptible to changes in the polypeptide chain conformation.[43] Since the proportion of α-helix to β-sheet domains of the protein was responsible for this peak symmetry, the deconvolution was performed by neglecting the contributions from other less ordered structures. From Amide I peak deconvolution (Figure S4) it could be seen that the α-helix to β-sheet ratio varied from pristine keratin to the nanocomposite. The β-sheet-to-α-helix peak area ratio varied from 1.8 to 4.6, indicating that a conformational change occurred upon the addition of the nanoparticles. nTiO$_2$ incorporation would inhibit a close packing of the keratin chains by reducing the degrees of freedom in the 3D conformation, limiting or even preventing the formation of crystalline regions. SEM images showed that the nTiO$_2$ were not agglomerated and distributed in the gel matrix as it was depicted in Figure S5 (Supplementary Information).

XRD analysis was performed to examine the crystallinity of the K hydrogel and K-TiO$_2$ hydrogels. Figure 2 showed the diffraction pattern of the semi-crystalline structure of K hydrogel with two peaks. The first one at 9.62° indicated the α-helix structure of keratin. The second one at 21° showed the β-sheet structure.[44] The nTiO$_2$ patterns revealed peaks corresponding to anatase (25.30°, 37.80° and 48.08°) and rutile (27.42°). This indicated that the nTiO$_2$ was a mixture of anatase and rutile phase.[45,46] As it had been stated in the introduction, the simultaneous presence of anatase and rutile phase nTiO$_2$ improved the photocatalytic activity compared to the individual components. The results showed that the composition was anatase 85% and rutile 15%. The introduction of nTiO$_2$ on polymeric matrices induced changes in the tridimensional polymeric network, producing changes on keratin diffraction peaks. This caused a reduction in intensity of keratin diffraction peaks when the nanoparticles were present in the composite. nTiO$_2$ incorporation would inhibit a close packing of the keratin chains by reducing the degrees of freedom in the 3D conformation, limiting or even preventing the formation of crystalline regions. These results would be related to those observed in the Raman. In the K-TiO$_2$ hydrogels patterns, four diffraction peaks at 25.30°, 27.42°, 37.80° and 48.08°
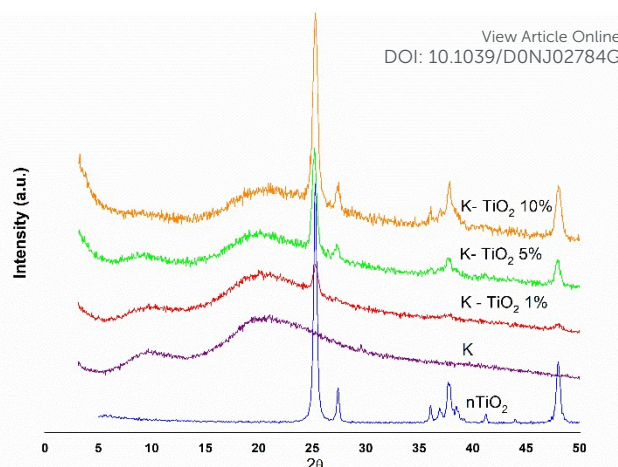

Figure 2. XRD spectra of the samples.

appeared, which were in agreement with the characteristic peaks of anatase and rutile form of TiO$_2$.[44] This meant that nTiO$_2$ crystalline structure was not affected by the incorporation in the keratin matrix. As the concentration (wt%) of nTiO$_2$ increased, the characteristic nTiO$_2$ peaks also increased and became the major peaks in the composites.

Dielectric spectroscopy (DS) provides information on the molecular dynamics by monitoring the relaxation processes. Figure 3 showed the DS spectra for the K and K-TiO$_2$ hydrogels. For all samples at low frequencies high permittivity values can be seen corresponding to interfacial polarization (also known as Maxwell-Wagner-Sillar effect). This type of polarization becomes from the limited displacement of free charges, such as ions, and their accumulation at interfacial areas, such as water-protein interfaces, when the different constituents of the material possess distinct permittivities [47]. The permittivity values at the low frequency region are higher for the K hydrogel than for the K-TiO$_2$ hydrogels. This decrease is probably due to the lower permittivity of TiO$_2$ in comparison with the water medium or its influence on the material dipole carriers [48]. From permittivity plots two main changes in the permittivity trend can be seen. One at the low frequency region and other at the high frequency region. The first would account for keratin segmental relaxation and the second would be due to local relaxations. From ε' and ε'' vs Frequency plots (Figure 3 A and B) it could be seen that the presence of nanoparticles influenced the relaxation processes of keratin in the hydrogel. The loss factor plot (Figure 3 C) showed a peak between 1-10 Hz that is shifted towards higher frequencies when TiO$_2$ is present, which was more evident at higher frequencies. Probably, the moieties capable of forming hydrogen bonds in the protein interacted with the TiO$_2$ surface, in particular with Ti-OH groups, which had faster relaxation dynamics. This effect had been reported for other hydrophilic polymers [49]. The Cole-Cole plot was obtained from the dependence ε' on ε'' on the complex plane and was presented in Figure 3 D. As could be seen, for all samples this plot presented two semicircles that were tilted toward the low frequency region (top-right). The two semicircles confirmed that two relaxation processes were taking place within the 0.1-1 MHz frequency range and that there was a contribution to the profile due to the bulk conductivity [50]. For the nanocomposites the bulk conductivity contribution was lower than for K hydrogels,
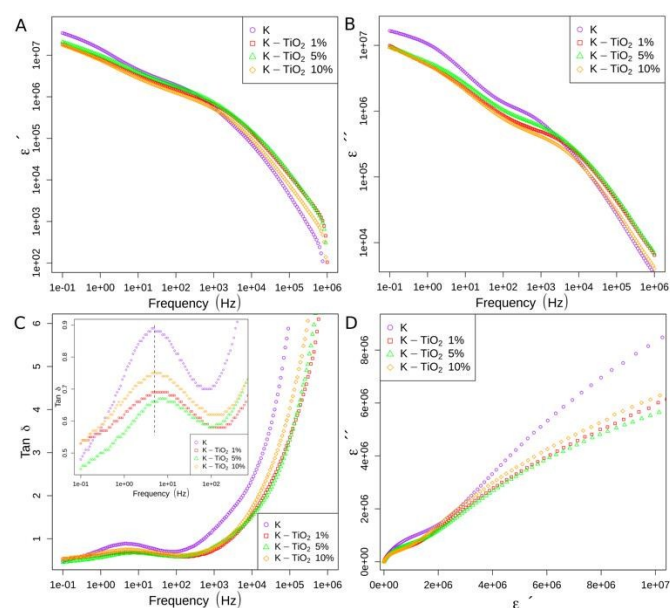
Figure 3. A) Real permittivity, B) Imaginary permittivity, C) Loss factor and D) Cole-Cole plot.

which was seen as lower values at the low frequency zone (top-right of the plot). This was probably related to a decrease in the free charge carriers in the matrix, as in the case of keratin ionized groups counterions. Both DS and Raman results confirmed that the nanoparticles had influence on keratin structural organization probably due to hydrogen bonding and keratin ionic groups interaction with the surface of the nanoparticle. As it is well known, the interaction of the surrounding media with the nanoparticle surface could have and impact in its photocatalytic performance.

Swelling
The hydrogel swelling was studied at different pH values (Figure S6). Both K and K-TiO$_2$ 10% presented different swelling values depending on the pH media, being low (around 150%) at low pH values (4 and 5) and higher since pH 6 (above 600%). The difference between pH 5 and 6 was significant for both hydrogels (p<0.05). The mechanism of this behaviour was established in a prior study. [51] As could be seen in Figure S6, as pH was increased from pH 6 to 7, the K hydrogels also increased their swelling. Neither K nor K-TiO$_2$ hydrogels presented significant differences between the swellings at pH 7 and 8 (p>0.05). Also, when comparing the swellings at pH 7 and at pH 8 it could be seen that there were significant differences (p<0.05) between K and K-TiO$_2$ hydrogel swellings showing lower swellings for the nanocomposites. This could be originated in a mobility restriction of keratin chains due to the ordering induced by the nanoparticles as was observed from FT-Raman and dielectric spectroscopy results.

Adsorption properties
Adsorption at different pH values
The dependence of pH on the adsorption of trimethoprim in the dark was shown in Figure 4. 1. It could be observed that for the tested samples (K, K-TiO$_2$ 10% and nTiO$_2$) there were no significant differences among the different assayed pH values (p> 0.05). These
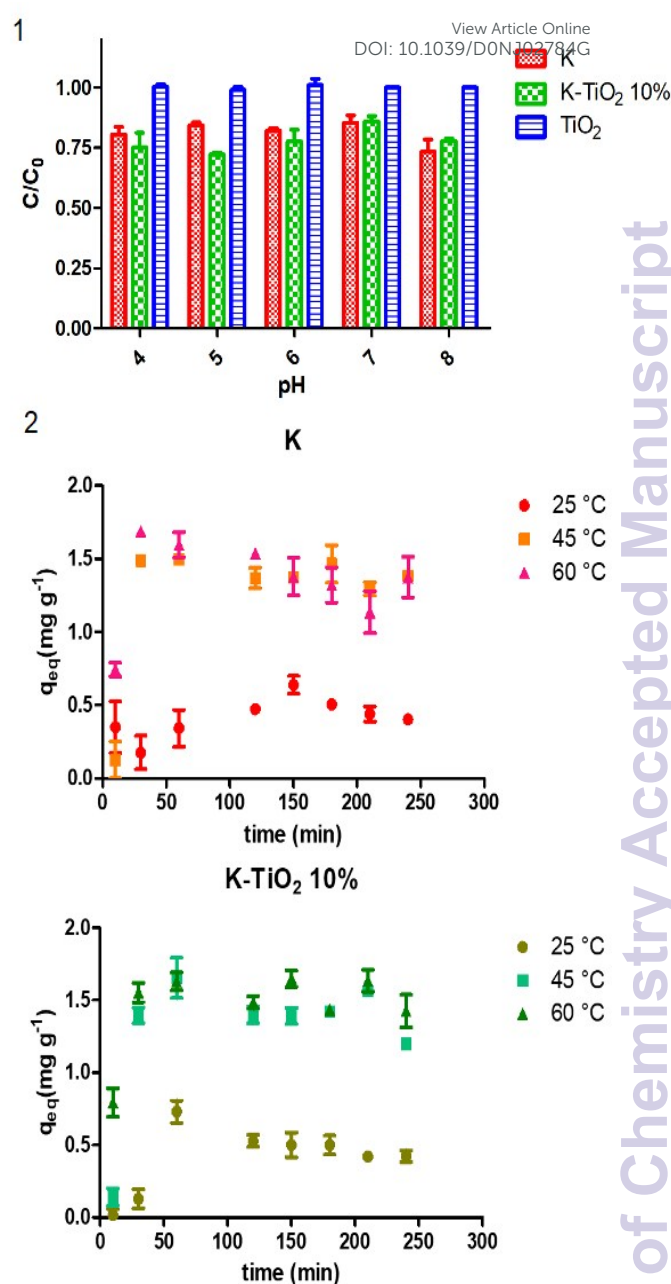
Figure 4. 1) Trimethoprim adsorption at different pH values. 2) Trimethoprim adsorption kinetics at different temperatures. C$_0$: initial trimethoprim concentration (0.172 mM), C: trimethoprim concentration after 18 h of interaction.

equilibrium uptake of trimethoprim to the hydrogel results showed that there was no relationship between the swelling, which was significantly higher at alkaline pH values, and the adsorption, hence the adsorption mechanism was due to chemical (ion exchange) and physical (H bonds, van der Waals) interactions between the active sites and the pollutant. Besides, no adsorption was observed in nTiO$_2$ in the different assayed pH values. Since these nanoparticles were non-porous [52] and the nTiO$_2$ surface was not prone to be altered or activated, i.e. by changing its surface charge, in the pH range tested, these nanoparticles would not be good adsorbents for

this type of organic molecule. Moreover, the TiO_2 surface would hardly be able to interact with trimethoprim by electrostatic attraction or by hydrophobic interactions.

Adsorption kinetics at different temperatures.

Trimethoprim adsorption was evaluated at different temperatures and time intervals. As shown in Figure 4. 2, equilibrium was achieved in 30 min when the temperatures were 45 and 60 °C, and remained constant until 240 min. At 25 °C a very low adsorption was verified during the time of the experiment. These results showed that the adsorption was temperature dependent. At higher temperatures a higher number of active cites were available to interact with trimethoprim molecules, indicating the adsorption process was endothermic. Thus, the extent of adsorption increased along with temperature.[53,54]

Photocurrent

Photocurrent determination was conducted to investigate the separation performance of photogenerated electron-hole pairs. Usually, the value of photocurrent indirectly represented the capacity of generating and transferring the photo-excited charge carrier, which related to the photocatalytic activity [20]. As shown in Figure 5, with the visible light turn on and off, the photocurrent

displayed a relatively stable trend, indicating that the electrons and holes generated by K-TiO_2 10% hydrogel could be separated during the degradation of the pollutant. Trimethoprim adsorption and photocatalytic degradation synergy by K-TiO_2 10% was also explored by photocurrent measurement. It could be observed that both TiO_2 and K-TiO_2 10% had a photoelectric response. The photocurrent of K-TiO_2 10% was enhanced in comparison with nTiO_2 sample. The enhanced photocurrent of the hydrogels may be due to the improved transition of photogenerated carriers via the porous network structure, these results are supported by the DS results. The porous network has been described in previous works.[23,55,56] In the K hydrogel the photocurrent presents negative values, contrasting with the theoretical expectation that for this sample the value of the photocurrent would be null. This effect could be awarded to electrolyte residues lodged in the anode, which upon receiving light can release electrons, that prompted by the potential will travel to the cathode, producing this negative current. Photoluminescence spectroscopy(PL) and optical absorption (OA) were used to examine the photoinduced charge carrier trapping, migration and transfer behaviour of semiconductor particles.[57] The photoluminescence emission spectrum of the TiO_2 was reported in a previous study of the group.[9] The luminescence spectrum of TiO_2 obtained using an excitation wavelength of 320 nm exhibits one main emission peaks at 375 nm. The emission band at 375 nm was due to the direct band to band transitions. The spectrum result of the photoluminescence signal depended mainly on the electron transition from the conduction band to the valence band. As it could be seen in Figure S7 in the Supplementary Information, no significant changes in the nTiO_2 absorption UV-Vis spectra was observed when they were immersed in the keratin hydrogel. The results from PL and OA would support the results obtained from the photocurrent assay from which it was proposed that the main responsible from enhanced photocurrent of the hydrogels may be due to the improved transition of photogenerated carriers via the porous network structure.
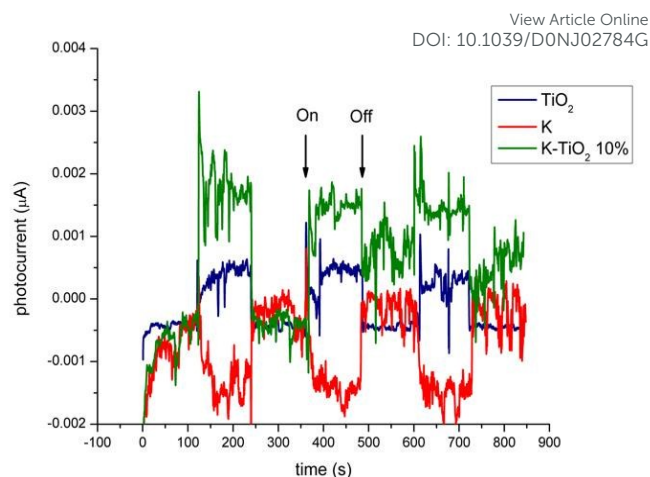

Figure 5. Photocurrent of the materials under light irradiation.

Degradation efficiency of Trimethoprim

To assess whether the photocatalysis was pH dependent, a solution of trimethoprim was treated with the different samples stabilized at different pH values and exposed to light for 2 h. In the results (Figure 6), it could be seen that in nTiO_2 there was no significant difference among the different assayed pH values ($p > 0.05$). Although the photocatalytic activity of a given material could be affected by the media pH, the nTiO_2 surface is not prone to change its surface characteristics in the pH range tested, thus, no difference between the pH values were observed. These results implied that the developed material would be useful at a wide range of pH values, diversifying the nature of the effluents to be treated. The decrease in trimethoprim concentration in the samples treated with K was due to the adsorption mechanism, in the nTiO_2, was only due to photocatalysis and in K-TiO_2 10% both mechanisms took place. The difference between nTiO_2 and K-TiO_2 10% may account for the lower diffusion of the pollutant in the hydrogel than in a solution.

Photocatalysis kinetic

The photocatalytic ability of K-TiO_2 10% hydrogel was studied by analyzing the remaining trimethoprim kinetics under visible light. As shown in Figure 6, this study was performed twice with the same material, each time with fresh trimethoprim solution. In the first experiment non significant difference was found between K and K-TiO_2. Thus, the main mechanism involved was adsorption and in the other one photocatalysis. In the adsorption process, a C/C_0 around 0.20 was achieved in both K and K-TiO_2 10% at 7 h of interaction time. In the second use of the materials, a difference was observed between the different treatments. In the K hydrogel a low decay was observed while in the K-TiO_2 a C/C_0 around 0.25 was achieved after 7 h interaction. In this case, photocatalysis was the predominant mechanism. In the first 2 h, trimethoprim in solution was rapidly degraded and then, the degradation rate decreased until equilibrium was achieved approximately in 7 h.

Taking into account the photocurrent experiment results (Figure 5), it would be expected that the K-TiO_2 10% performance would be better than the nTiO_2. However, in the pollutant degradation studies (Figure 6), no significant difference could be found between

ARTICLE

them ($p>0.05$). This could have been due to the difficulty in the diffusion of the involved chemical species in the gel matrix. The apparent first-order kinetic model that was derived from the Langmuir–Hinshelwood kinetic equation was used in this study to determine the photocatalytic degradability of the trimethoprim and was described in the Supplementary Information.[9] The apparent first-order rate constant (k_{app} in h^{-1}), equivalent to the slope of the linear regression was applied to evaluate the photocatalytic degradation rates of K-TiO$_2$ 10%. In Figure S8 (Supplementary Informationn) the plotting $\ln C_0/C$ as a function of reaction time yielded a straight line for the second cycle demonstrating that the degradation follows the apparent first-order kinetic law and confirming trimethoprim decomposition due to photocatalysis. However, the fit did not converge for the first cycle probably because of the relevant contribution of the adsorption step.

Comparison between different materials and reuse.
Hydrogels prepared with different content of nTiO$_2$, K-TiO$_2$ 1%, K-TiO$_2$ 5% and K-TiO$_2$ 10%, degradation efficiency was evaluated at 4 h interaction time at 25 °C. Higher concentrations were not assayed since the obtained hydrogels were too brittle to manipulate. The remaining trimethoprim was significantly lower in K-TiO$_2$ 10% than in K-TiO$_2$ 1% and K-TiO$_2$ 5% ($p<0.05$) (Figure 4). These results proved that increasing the photocatalyst concentration provided higher photocatalytic efficiencies. This suggested that the K-TiO$_2$ 10% was the appropriate material for trimethoprim remediation.
This assay was repeated 4 times with fresh trimethoprim solution each time. There was no significant difference between the use number and the C/C_0 ($p>0.05$), showing that the efficiency of the developed material was maintained during at least 4 cycles and therefore these nanocomposites have suitable reusability.
As it was established in the Introduction, immobilized photocatalytic systems presented many advantages for water decontamination processes. The stability of the immobilized photocatalyst was reported as a key factor in the development of these materials since the loss of the photocatalytic particles into the water decreased the photocatalytic performance of the process. In the K-TiO2 hydrogel there was no significant difference among the different cycles, showing that the developed material presented good stability.

Conclusions

In this work, a keratin hydrogel containing nTiO$_2$ with photocatalytic activity was developed. This material was characterized and its efficiency in the degradation of the emergent contaminant trimethoprim was evaluated. The spectroscopic results showed the typical signals of the materials and proved the presence of the nTiO$_2$ immersed in the 3D hydrogel. These hydrogels showed the ability to adsorb and degrade trimethoprim in the presence of UV-Visible light in batch conditions. Experimental variables (time, temperature, pH) were varied in order to characterize the material performance. The equilibrium uptake of trimethoprim to the hydrogel was endothermic, it was achieved within 30 min and no dependence of pH was found. The photocatalytic activity was also not influenced by the pH of the media. In the K-TiO$_2$ samples, the mechanism involved in the decrease of trimethoprim concentration
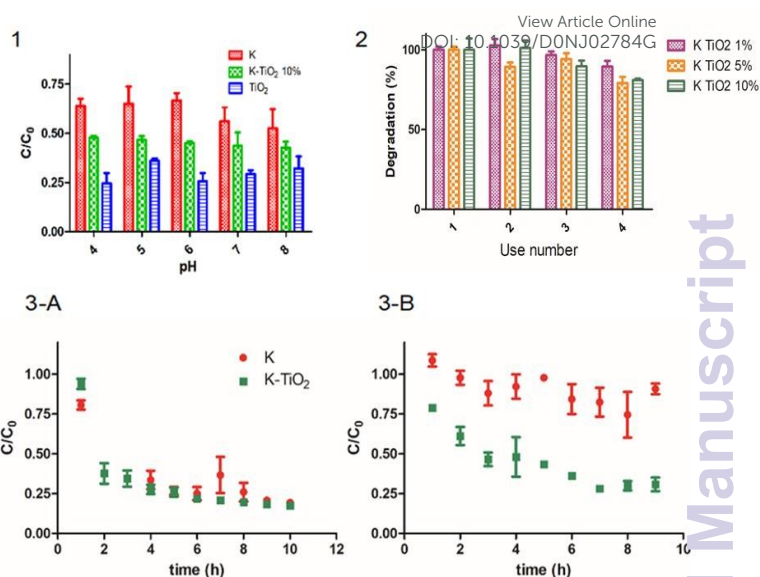

Figure 6. 1) Remaining trimethoprim after light irradiation at different pH values. 2) 2) Degradation % of TMP after light irradiation at different number of uses. Degradation % of cycle 1 was considered 100%. 3) Remaining trimethoprim after light irradiation at different times A) First cycle and B) second cycle.

were adsorption and photocatalysis while in K samples only adsorption was the responsible. The K-TiO$_2$ samples could be reused for at least 4 times maintaining a similar efficiency. When performing the photocurrent tests, it was observed that it was greater in the hydrogels than in the nanoparticles. However, in the photocatalysis analysis, the decrease in trimethoprim concentration was equivalent in both treatments. This unexpected difference may be due to the lower diffusion of the pollutant in the hydrogel matrix. Nevertheless, the hydrogels had the advantage of its easy handle and subsequent reuse compared with nTiO$_2$

Conflicts of interest
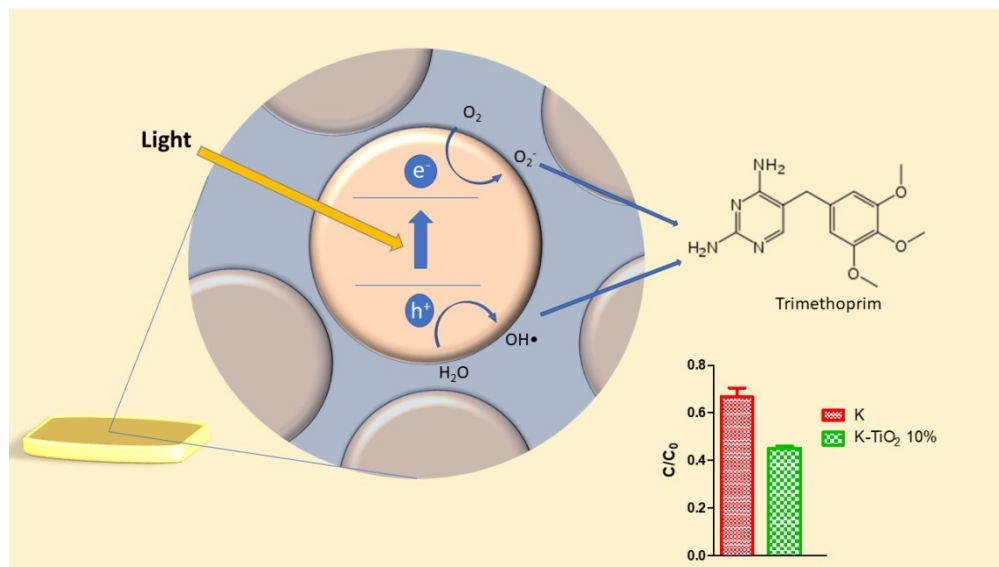
There are no conflicts to declare.

Acknowledgements

Notes and references

1   D. Bunke, S. Moritz, W. Brack, D. L. Herráez, L. Posthuma and M. Nuss, *Environmental Sciences Europe*, 2019, **31**, 32.
2   V. Dulio, B. Van Bavel, E. Brorström-Lundén, J. Harmsen, J. Hollender, M. Schlabach, J. Slobodnik, K. Thomas and J. Koschorreck, *Environmental Sciences Europe*, 2018, **30**, 5.
3   Z. Visanji, S. Sadr, M. Johns, D. Savic and F. A. Memon, International Hydroinformatics Conference, 2018.
4   M. Gavrilescu, K. Demnerová, J. Aamand, S. Agathos and F. Fava, *New Biotechnology*, 2015, **32**, 147–156.
5   R. Rosal, A. Rodríguez, J. A. Perdigón-Melón, A. Petre, E. García-Calvo, M. J. Gómez, A. Agüera and A. R. Fernández-Alba,

Water research, 2010, **44**, 578–588.

6   F. Hernández, N. Calisto-Ulloa, C. Gómez-Fuentes, M. Gómez, J. Ferrer, G. González-Rocha, H. Bello-Toledo, A. Botero-Coy, C. Boix and M. Ibáñez, *Journal of hazardous materials*, 2019, **363**, 447–456.

7   J. Martínez-Costa, M. M. Rubio and R. Leyva-Ramos, *Catalysis Today*, 2020, **341**, 26–36.

8   A. Bernabeu, R. F. Vercher, L. Santos-Juanes, P. J. Simón, C. Lardín, M. A. Martínez, J. A. Vicente, R. González, C. Llosá, A. Arques and A. M. Amat, *Catalysis Today*, 2011, **161**, 235–240.

9   M. E. Villanueva, G. J. Copello and V. C. Dall'Orto, *New Journal of Chemistry*, 2018, **42**, 15405–15412.

10 F. Wesarg, F. Schlott, J. Grabow, H.-D. Kurland, N. Heßler, D. Kralisch and F. A. Müller, *Langmuir*, 2012, **28**, 13518–13525.

11 Q. Cai and J. Hu, *Journal of hazardous materials*, 2017, **323**, 527–536.

12 M. Ghosh, M. Lohrasbi, S. S. Chuang and S. C. Jana, *ChemCatChem*, 2016, **8**, 2525–2535.

13 M. Abellán, J. Giménez and S. Esplugas, *Catalysis Today*, 2009, **144**, 131–136.

14 I. Michael, E. Hapeshi, V. Osorio, S. Perez, M. Petrovic, A. Zapata, S. Malato, D. Barceló and D. Fatta-Kassinos, *Science of the total environment*, 2012, **430**, 167–173.

15 W. H. Abdelraheem, M. K. Patil, M. N. Nadagouda and D. D. Dionysiou, *Applied Catalysis B: Environmental*, 2019, **241**, 598–611.

16 A. Giampiccolo, D. M. Tobaldi, S. G. Leonardi, B. J. Murdoch, M. P. Seabra, M. P. Ansell, G. Neri and R. J. Ball, *Applied Catalysis B: Environmental*, 2019, **243**, 183–194.

17 T. Kawahara, Y. Konishi, H. Tada, N. Tohge, J. Nishii and S. Ito, *Angewandte Chemie International Edition*, 2002, **41**, 2811–2813.

18 T. Ohno, K. Sarukawa, K. Tokieda and M. Matsumura, *Journal of Catalysis*, 2001, **203**, 82–86.

19 X. Chen, Q. Chen, W. Jiang, Z. Wei and Y. Zhu, *Applied Catalysis B: Environmental*, 2017, **211**, 106–113.

20 J. Yang, Z. Li and H. Zhu, *Applied Catalysis B: Environmental*, 2017, **217**, 603–614.

21 M. Zhang, W. Jiang, D. Liu, J. Wang, Y. Liu, Y. Zhu and Y. Zhu, *Applied Catalysis B: Environmental*, 2016, **183**, 263–268.

22 M. Zhang, W. Luo, Z. Wei, W. Jiang, D. Liu and Y. Zhu, *Applied Catalysis B: Environmental*, 2016, **194**, 105–110.

23 G. Galaburri, M. L. P. Ramos, J. M. Lázaro-Martínez, R. F. de Luis, M. I. Arriortua, M. E. Villanueva and G. J. Copello, *European Polymer Journal*, 2019, **118**, 1–9.

24 T. R. Ham, R. T. Lee, S. Han, S. Haque, Y. Vodovotz, J. Gu, L. R. Burnett, S. Tomblyn and J. M. Saul, *Biomacromolecules*, 2015, **17**, 225–236.

25 M. E. Villanueva, M. L. Cuestas, C. J. Pérez, V. C. Dall and G. J. Copello, *Journal of colloid and interface science*, 2019, **536**, 372–380.

26 Z. Davoudi, M. Rabiee, B. Houshmand, N. Eslahi, K. Khoshroo, M. Rasoulianboroujeni, M. Tahriri and L. Tayebi, *Drug development and industrial pharmacy*, 2018, **44**, 40–55.

27 T. Posati, D. Giuri, M. Nocchetti, A. Sagnella, M. Gariboldi, C. Ferroni, G. Sotgiu, G. Varchi, R. Zamboni and A. Aluigi, *European Polymer Journal*, 2018, **105**, 177–185.

28 M. Zhai, Y. Xu, B. Zhou and W. Jing, *Journal of Photochemistry and Photobiology B: Biology*, 2018, **180**, 253–258.

29 M. W. Donner, M. Arshad, A. Ullah and T. Siddique, *Science of The Total Environment*, 2019, **647**, 1539–1546.

30 S. Z. Mousavi, M. Manteghian, S. A. Shojaosadati and H. Pahlavanzadeh, *Advances in Environmental Technology*, 2018, **4**, 83–93.

31 S. Saha, M. Zubair, M. Khosa, S. Song and A. Ullah, *Journal of Polymers and the Environment*, 2019, 1–15.

32 L. Chen, Z. Jia, Y. Tang, L. Wu, Y. Luo and D. Jia, *Composites Science and Technology*, 2017, **144**, 11–17.

33 Y. Song and Q. Zheng, *Progress in Materials Science*, 2016, **84**, 1–58.

34 J. Zhao, J. Yin, J. Zhong, T. Jiao, Z. Bai, S. Wang, L. Zhang and Q. Peng, *Nanotechnology*, 2019, **31**, 085603.

35 Y. Feng, J. Yin, S. Liu, Y. Wang, B. Li and T. Jiao, *ACS Omega*, 2020, **5**, 3725–3733.

36 J. Zhu, R. Wang, R. Geng, X. Zhang, F. Wang, T. Jiao, J. Yang, Z. Bai and Q. Peng, *RSC advances*, 2019, **9**, 22551–22558.

37 M. Wojdyr, *Journal of Applied Crystallography*, 2010, **43**, 1126–1128.

38 R. Paquin and P. Colomban, *Journal of Raman Spectroscopy: An International Journal for Original Work in all Aspects of Raman Spectroscopy, Including Higher Order Processes, and also Brillouin and Rayleigh Scattering*, 2007, **38**, 504–514.

39 K. Dai, T. Peng, D. Ke and B. Wei, *Nanotechnology*, 2009, **20**, 125603.

40 M. Hamadanian, A. Reisi-Vanani and A. Majedi, *Journal of the Iranian Chemical Society*, 2010, **7**, S52–S58.

41 W. Su, J. Zhang, Z. Feng, T. Chen, P. Ying and C. Li, *The Journal of Physical Chemistry C*, 2008, **112**, 7710–7716.

42 J. Shao, J. Zheng, J. Liu and C. M. Carr, *Journal of Applied Polymer Science*, 2005, **96**, 1999–2004.

43 H. G. M. Edwards, D. E. Hunt and M. G. Sibley, *Spectrochimica Acta Part A: Molecular and Biomolecular Spectroscopy*, 1998, **54**, 745–757.

44 H. Y. Zhu, J. A. Orthman, J.-Y. Li, J.-C. Zhao, G. J. Churchman and E. F. Vansant, *Chem. Mater.*, 2002, **14**, 5037–5044.

45 M. Ghosh, J. Liu, S. S. Chuang and S. C. Jana, *ChemCatChem*, 2018, **10**, 3305–3318.

46 D. Wu, M. Yi, H. Duan, J. Xu and Q. Wang, *Carbon*, 2016, **108**, 394–403.

47 F. Bibi, M. Villain, C. Guillaume, B. Sorli and N. Gontard, *Sensors*, 2016, **16**, 1232.

48 A. Wypych, I. Bobowska, M. Tracz, A. Opasinska, S. Kadlubowski, A. Krzywania-Kaliszewska, J. Grobelny and P. Wojciechowski, *Journal of Nanomaterials*, 2014, **2014**, 1–9.

49 R. J. Sengwa, S. Choudhary and S. Sankhla, *Colloids and Surfaces A: Physicochemical and Engineering Aspects*, 2009, **336**, 79–87.

50 A. El Nahrawy, A. Abou Hammad, G. Turky, M. Elnasharty and A. Youssef, *Intl J Adv Eng, Technol Comput Sci*, 2015, **2**, 9–14.

51 M. L. P. Ramos, J. A. González, L. Fabian, C. J. Pérez, M. E. Villanueva and G. J. Copello, *Materials Science and Engineering: C*, 2017, **78**, 619–626.

52 M. Ovcharov, V. Shvalagin, N. Shcherban, M. Nazarkovskii and V. Granchak, *Theoretical and Experimental Chemistry*, 2013, **49**, 172–177.

53 Z. Aksu, *Separation and Purification Technology*, 2001, **21**, 285–294.

54 Y. Ho, C. Huang and H. Huang, *Process Biochemistry*, 2002, **37**, 1421–1430.

55 M. L. P. Ramos, J. A. González, L. Fabian, C. J. Pérez, M. E. Villanueva and G. J. Copello, *Materials Science and Engineering: C*, 2017, **78**, 619–626.

56 M. L. P. Ramos, G. Galaburri, J. A. González, C. J. Pérez, M. E. Villanueva and G. J. Copello, *Journal of environmental chemical engineering*, 2018, **6**, 7021–7028.

57 Z. Liu, D. D. Sun, P. Guo and J. O. Leckie, *Nano letters*, 2007, **7**, 1081–1085.

338x190mm (96 x 96 DPI)